Defence Technology xxx (xxxx) xxx

Contents lists available at ScienceDirect

Defence Technology

journal homepage: www.keaipublishing.com/en/journals/defence-technology

Shock wave mitigation using zig-zag structures and cylindrical obstructions

Arun Kumar R*, Vaibhav Pathak

Department of Mechanical Engineering, Indian Institute of Technology Jodhpur (IITJ), Jodhpur, Rajasthan, 342037, India

ARTICLE INFO

Article history:
Received 10 May 2020
Received in revised form
16 September 2020
Accepted 16 October 2020
Available online xxx

Keywords:
Blast wave mitigation
Blockage ratio
Geometric obstructions
Shock wave reflection and diffraction
Zig-zag structure

ABSTRACT

The present study focuses on the mitigation of shock wave using novel geometric passages in the flow field. The strategy is to produce multiple shock reflections and diffractions in the passage with minimum flow obstruction, which in turn is expected to reduce the shock wave strength at the target location. In the present study the interaction of a plane shock front (generated from a shock tube) with various geometric designs such as, 1) zig-zag geometric passage, 2) staggered cylindrical obstructions and 3) zig-zag passage with cylindrical obstructions have been investigated using computational technique. It is seen from the numerical simulation that, among the various designs, the maximum shock attenuation is produced by the zig-zag passage with cylindrical obstructions which is then followed by zig-zag passage and staggered cylindrical obstructions. A comprehensive investigation on the shock wave reflection and diffraction phenomena happening in the proposed complex passages have also been carried out. In the new zig-zag design, the initial shock wave undergoes shock wave reflection and diffraction process which swaps alternatively as the shock front moves from one turn to the other turn. This cyclic shock reflection and diffraction process helps in diffusing the shock wave energy with practically no obstruction to the flow field. It is found that by combining the shock attenuation ability of zig-zag passage (using shock reflection and diffraction) with the shock attenuation ability of cylindrical blocks (by flow obstruction), a drastic attenuation in shock strength can be achieved with moderate level of flow blocking.

1. Introduction

It is well known that a rapid release of energy from a localized space, like in an explosion, creates a high-intensity pressure wave called the blast wave. Blast wave consists of a moving shock front, followed by a high impulse blast wind [1]. The overpressure behind the shock front and the blast wind can cause severe damage to humans, structures, and equipment [2]. Recent studies have also shown that the shock wave interaction with humans can lead to damage of internal organs without the occurrence of any external physical impairment [3,4]. Studies have shown that even a fairly weak shock wave can cause mild traumatic brain injury (MTBI) without a direct blow to the head [5–7]. Therefore, considering the catastrophic effects of the shock wave to both humans and civil structures, it is important to mitigate the shock strength to a level where the damage can be reduced to a certain extent.

In recent times much interest has been shown in designing better shock mitigation strategies, especially in military applications like bunkers, military vehicles, helmets, bomb suits, etc. One of the major shock attenuation strategies is to reduce the incident shock strength before it hits the target [8]. The most prominent of these methods is to use geometric blockages [9–14] in the flow passage ahead of the target which produces shock reflection and attenuates the shock strength. In the past, various geometric blockages like grids and orifice plates [9,10], perforated plates [11], arrayed baffle plates [12], matrices of solid obstacles of various shapes [13,14], etc. were investigated, and it was reported that a fairly good shock attenuation could be achieved based on the flow passage created by these blockages. Fig. 1(a) to Fig. 1(e) shows the schematic of the prominent geometric obstruction patterns investigated in the past. Apart from shock wave reflection, shock

* Corresponding author. Dept. of Mechanical Engg. Indian Institute of Technology Jodhpur, India.
E-mail address: arunkr@iitj.ac.in (A. Kumar R).
Peer review under responsibility of China Ordnance Society

https://doi.org/10.1016/j.dt.2020.10.001

Please cite this article as: A. Kumar R and V. Pathak, Shock wave mitigation using zig-zag structures and cylindrical obstructions, Defence Technology, https://doi.org/10.1016/j.dt.2020.10.001

Nomenclatures

BR	Blockage Ratio
BTBI	Blast-induced Traumatic Brain Injury
CFD	Computational Fluid Dynamics
DSW	Diffracted Shock Wave
FDS	Flux-Difference Splitting
ISW	Initial Shock Wave
MTBI	Mild Traumatic Brain Injury
ms	milli second
RSW	Reflected Shock Wave
SMR	Simple Mach Reflection
SST	Shear Stress Transport
SSW	Secondary Shock Wave
TSW	Transmitted Shock Wave
t	Time
A_0	Un-obstructed initial shock tube area
A_b	Projected obstruction area
M_s	Shock Wave Mach number
P_1	Pressure at driven section
P_4	Pressure at driver section

diffraction can also help in diffusing the shock wave energy. Igra et al. [15] investigated this aspect by considering a double bend geometric structure, as shown in Fig. 1(f), and considerable shock wave mitigation was reported in their study.

Another method to attenuate the shock impact is to coat the target material with shock-absorbing materials. Studies have shown that materials with porous structure (like porous compressible foams) undergo plastic deformation and thereby exhibit greater shock-absorbing capacity [16–18]. Sommerfeld [19] proposed that the presence of small solid particles or liquid droplets into the gaseous phase also mitigates the shock wave strength. Bakken et al. investigated the effect of granular filters in attenuating shock strength [20]. Sembian et al. [21] reported that the use of aqueous foam barriers could produce significant shock wave attenuation. Several studies reported that polymer foams (such as polyurethane foams or polystyrene foams) exhibit better shock-absorbing capacity due to the collapse of the internal cell structures under impact loading [22–24]. Few studies explored the use of novel building material in developing blast resistance structures such as using ultra-high-performance fiber-reinforced self-compacting concrete [25], reinforced concrete panels with waste steel fibers [26], composite structural configurations like aluminum foam layer inside two layers of concrete [27], etc. A comprehensive review of the existing methods (based on geometrical blocking and shock absorbing coatings) to mitigate the shock strength can be found in the report by Igra et al. [28].

It should be noted that even though these studies were promising, much work is still needed, especially in designing more effective geometric passage and shock attenuating materials. Most of the existing strategies for blast attenuation use geometric obstructions placed on the blast path, which blocks the shock wave by producing shock wave reflection. However, the shock attenuation

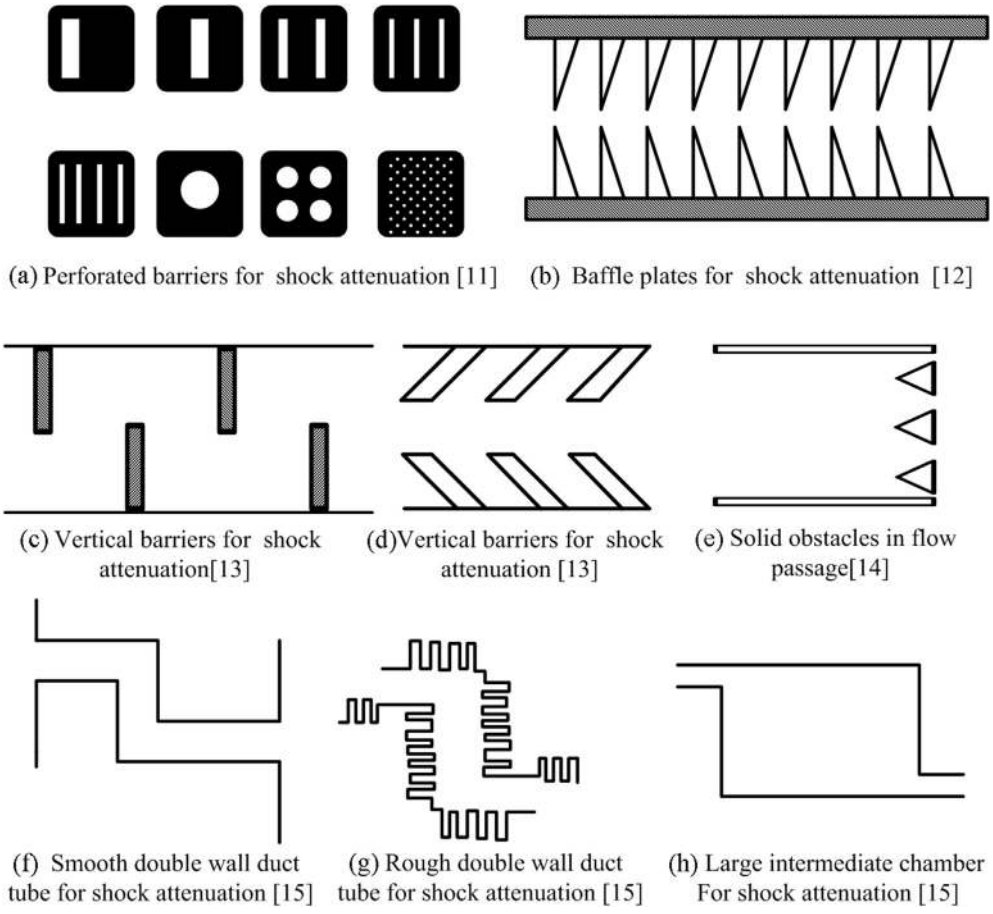

Fig. 1. Schematic of few prominent previous geometric designs for shock attenuation.

based on geometric obstructions will be effective only if the blockage area to the flow is quite large. In order to increase the blockage area, the entire blast path should be packed with sufficiently large quantity of solid obstructions which naturally increases the weight of the protective structure. In the present study, an attempt is made to investigate a new geometric design with minimum flow obstruction by using a zig-zag passage in the blast path. Unlike the geometric structure based on solid obstructions, the zig zag structure is mostly hollow with minimum blockage to the flow, which naturally reduces the weight of the protective structure. The shock attenuation is achieved through the multiple shock reflections happening at the foot of the shock wave rather than the entire shock wave reflected by the solid blocks. It is also expected that a combination of the zig-zag structure with few conventional solid obstructions placed in the zig-zag passage will produce a drastic shock attenuation compared to the shock attenuation produced by the highly packed solid obstructions alone. Hence a new design with few cylindrical obstructions placed in the zig-zag structure has also been investigated and its shock attenuation characteristics have been compared to the case with only staggered cylindrical obstruction placed in the flow field. It is also seen from literature that the fluid dynamics study on the unsteady shock reflections over complex geometric blockages are still not properly investigated and is an active area of research. Hence, a comprehensive investigation on the shock reflection patterns with complex geometric obstructions have also been carried out in the present study. The major aspects of the present study are thus two-fold. The first aspect is to check the general shock attenuation characteristics with the new geometric designs. The second aspect is to understand the shock reflection and diffraction characteristics with complex structures.

2. Computational schemes

In the present work, computational fluid dynamics (CFD) simulation has been carried out to investigate the effect of various geometric passages on shock attenuation. In order to simulate an initial plane shock front, a shock tube simulation has been employed. The computational domain for the shock tube consists of a driver section (high-pressure region) of 1000 mm length and a driven section (low pressure) of 1000 mm length, as shown in Fig. 2 (a). The driver and driven section are separated by a diaphragm. The driver section is initialized with the pressure of 15 bar, and the driven section is initialized with 1 bar. Both the driver and driven sections were initialized with a temperature of 300 K. Air was considered as the working gas for both driver and driven gas. An instantaneous rupture of diaphragm is assumed for the present simulation. The flow field is numerically solved using two dimensional transient compressible Reynolds average Navier-Stokes equations (URANS), using a commercial CFD package ANSYS FLUENT 2019 R2. The flow turbulence was modeled using SST $k-\omega$ model, which is basically a RANS-based method. In SST $k-\omega$ model, the turbulent viscosity used for the computation of Reynolds stress tensor is calculated by solving the transport equation for turbulent kinetic energy (k) and the specific dissipation rate (ω). The working gas is considered as ideal gas to account for the density variation and viscosity variation with respect to temperature was modeled using Sutherland's approach. The cell-centered solutions are extrapolated to the face centers by using second order upwind scheme. The flux crossing the cell boundaries are computed using Roe-flux difference splitting scheme. The time integration for the governing equation was carried out using second-order implicit schemes. The time step used for the simulation is 10^{-8} s with ten inner loop iterations per time step. The governing flow equations were solved in the coupled form (density-based solver available in Fluent software). The details of the computational methods used for the current simulation are given in Table 1.

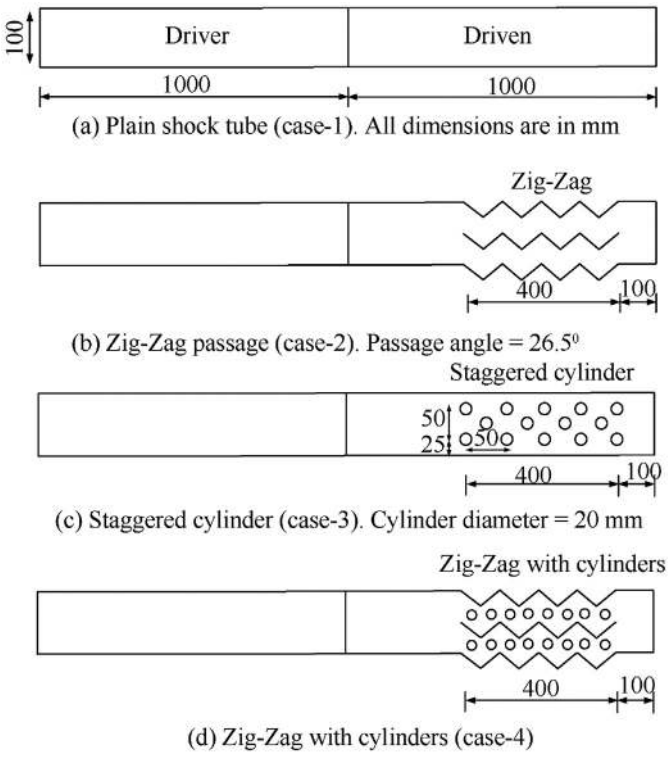

Fig. 2. Computational domain for various shock attenuation designs.

In the present study, various geometric designs for shock wave attenuation, as shown in Table 2, have been investigated. CFD simulations have been performed with various geometric passages at the downstream side of the driven section. The computational domains of various geometric cases are shown in Fig. 2 (b), 2(c), and 2(d). For all the cases, the length of the driven section over which geometric modifications have been employed is kept constant. The blockage ratio (BR), which is defined as the ratio of the projected obstruction area (A_b) to the un-obstructed initial shock tube area (A_0), produced by various cases have also been computed, and a schematic of this is shown in Fig. 3. It should be noted that the degree of shock wave attenuation produced by the new design (zig-zag passage) primarily depends on the wedge angle at each pass and the passage length. However, in the present study, a parametric study on optimizing these geometric parameters have not been attempted since this itself is a rigorous work with the requirement of many CFD simulation with various geometric models. The major objectives of the present study are thus limited only to investigate the effectiveness of the new designs and its shock reflection characteristics.

Table 1
Computational details.

Spatial discretization	Second order
Transient formulation	Second order implicit
Flux discretization	Roe-FDS
Time step	10^{-8} s
Turbulence model	SST k-ω
Density of air	Ideal gas equation
P_4/P_1	15
Working Medium	Air

Table 2
Various geometric designs to attenuate shock wave.

Cases	Blockage Ratio (BR)
Plain shock tube (Case-1)	0
Zig-Zag (Case-2)	0
Staggered cylinders (Case-3)	0.6
Zig-Zag with cylinders (Case-4)	0.4

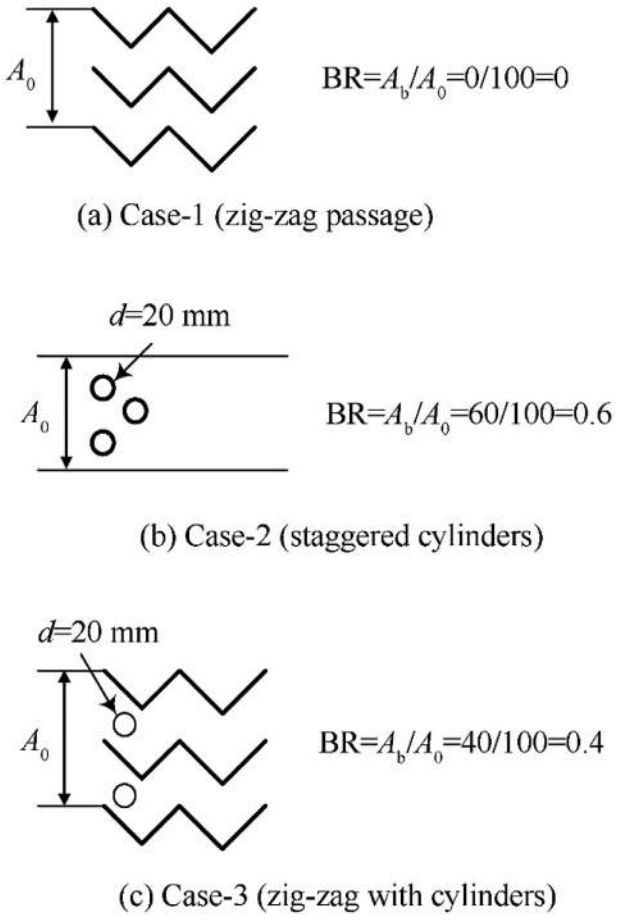

Fig. 3. Schematic showing the blockage ratio for various cases.

2.1. Mesh independence study

In order to find an optimum mesh size, a mesh independence study has been carried out by considering the plain shock tube simulation with various grid sizes. For the mesh independence study, the shock tube simulations with four grid distributions (1500, 2000, 2500, and 3000 nodes) at the driven section have been carried out. The computational domain has been discretized using quadrilateral cells with simulation conditions same as given in Table.1. Fig. 4(a) shows the pressure distribution along the centreline for various grid cases at a time instant of 0.05 ms. It is clearly evident from the centreline pressure plot that the solution does not vary much with all the grid systems considered in the present study. For better clarity, the centreline pressure variation close to the shock front has been zoomed and is shown in Fig. 4(b). The shock overpressure plot shown in Fig. 4(b) clearly shows that the solution does not vary much with the increase in mesh count above 2500 nodes in the driven section, implying a mesh independent solution. For the plain shock tube case, 2500 nodes in the driven section correspond to each cell representing a physical length of 0.4 mm. For all other geometric case simulations, the grid distribution is chosen such that an individual cell should represent at least 0.4 mm, which is the cell size corresponding to the mesh independent solution obtained for the plain shock tube case.

2.2. Validation

In the present study, the CFD code has been validated with two experimental studies. The first validation case was carried out with the experimental study of a plain shock tube conducted by Reddy et al. [29]. The second validation case was carried out with the experimental study of Igra et al. [15] in which the shock wave diffraction and subsequent shock wave attenuation produced by a large intermediate chamber placed in the shock path was investigated.

In the shock tube experiment, the shock overpressure at various measuring points have been monitored which in turn is used to determine the shock arrival time at predefined locations and thereby the shock wave Mach number. The schematic of the experimental geometry is shown in the inset in Fig. 5. The experiments have been conducted for various diaphragm pressure ratios (P_4/P_1) and the corresponding shock wave Mach numbers have been evaluated. CFD simulations have been performed with various diaphragm pressure ratios used in the experiment and the corresponding Mach numbers have been predicted. Fig. 5 shows the comparison of the computed Mach numbers for various pressure ratios and their corresponding experimental values. It is clearly evident from the first validation simulation that the present CFD code agrees well with the prediction of shock wave Mach number in shock tube flows.

The second validation case has been performed on a more specific case which involves complex shock diffraction and reflection processes. The geometrical details of the experimental study are shown in the inset in Fig. 6. The experimental study reported the shock diffraction patterns at various time instants and the pressure histories at four different measuring locations (as shown in Fig. 6). For the validation purpose, the shock pressure jump at each measuring locations has been extracted from the experimental pressure history and has been compared with the CFD predicted shock pressure jump at the same locations. For both the experimental and CFD studies, the time $t = 0$ is taken as the time instant at which shock wave just moves over the first pressure sensor (P_1). This will ensure to compare the shock arrival time from one sensor to the other sensor from the CFD and experimental studies. The shock pressure jump data predicted from CFD, as shown in Fig. 6, shows a close match with the experimental data. Moreover, the shock arrival time at various measuring location predicted from CFD also shows close resemblance with the experimental data.

The experimental study also investigated the shock wave diffraction and reflection using schlieren imaging technique. Schlieren imaging is an optical measurement technique which captures the density gradients in the flow field. In Schlieren imaging technique, a parallel beam of light is passed through the test section and its image formed by a lens/mirror system is captured using a high speed camera. When there is a density gradient in the flow filed, the light bends and the deflected rays will be either blocked or passed by a knife edge which gives a dark or bright contrast change in the test section image. This technique is particularly useful to study the shock wave structures which produce a sharp density jump in the flow field. Further details on schlieren techniques can be found in the monograph by Settles [31]. Fig. 7(a) to 7(d) shows the numerical schlieren predicted from the CFD code and its comparison with the experimental schlieren

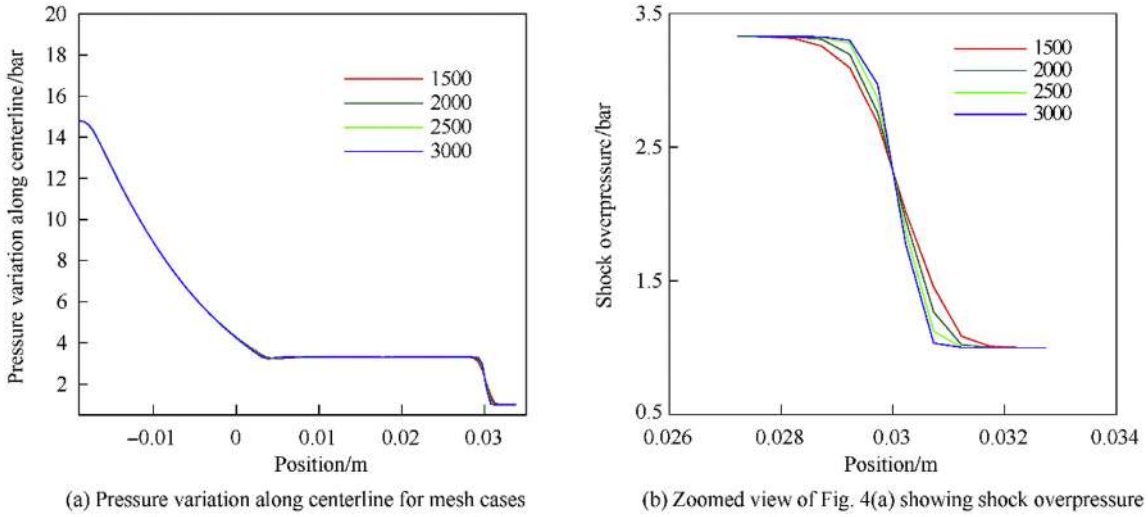

(a) Pressure variation along centerline for mesh cases

(b) Zoomed view of Fig. 4(a) showing shock overpressure

Fig. 4. Pressure distribution along the centerline for the plain shock tube case with various grid distributions (t = 0.05 ms).

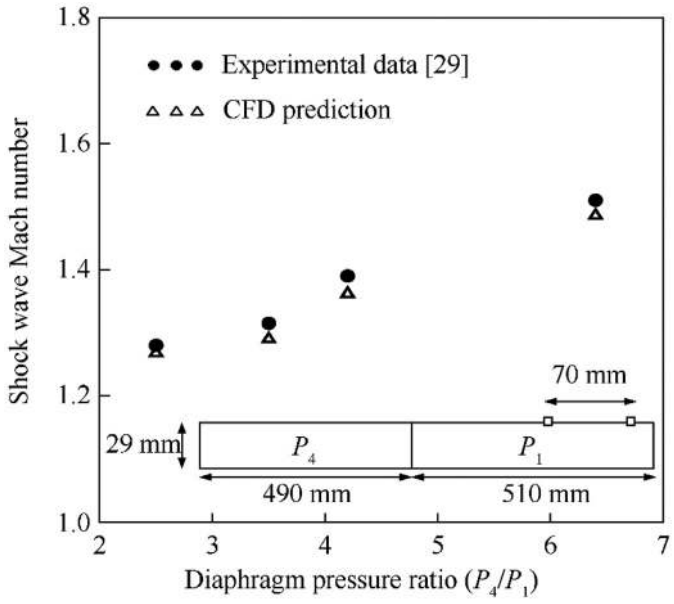

Fig. 5. Experimental and CFD comparison of shock wave Mach number for various diaphragm pressure ratios (P_4/P_1) in a plain shock tube.

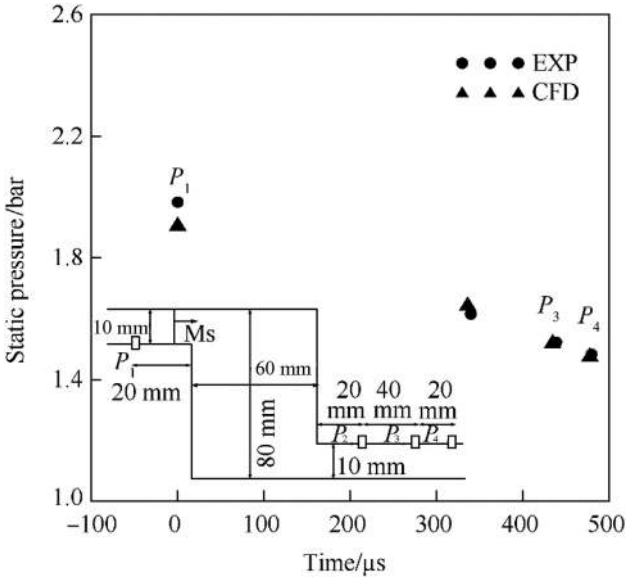

Fig. 6. Comparison of CFD predicted and experimentally measured [15] shock pressure jumps at various measuring locations. P_1 = 0.987 bar, T_1 = 23.4 °C and M_s = 1.3466.

images. The numerical schlieren images are computed by finding the gradient of density field using ParaView software. For this qualitative comparison, the experimental frame at which the shock wave just diffracts into the large intermediate section has been considered as t = 0. This ensures a common starting reference time for the qualitative comparison of both the CFD and experimental case. It is clearly seen from Fig. 7(a) to 7(d), that the various flow features like, the shock diffraction, primary vortex, shock reflections etc. predicted by the CFD shows close resemblance with the experimental data. The validation study thus clearly shows that the present CFD code is capable enough to predict complex shock diffraction and reflection patters with good accuracy.

3. Results and discussion

This section consists of two parts. In the first part, the shock attenuation effects produced by various geometric designs are compared. In the second part, a detailed investigation on the complex fluid dynamics (particularly on the shock reflection and diffraction characteristics) involved in various geometric designs have been reported.

3.1. Shock attenuation comparison for various designs

In the present study, three major parameters were investigated to compare the shock wave attenuation effect produced by various geometric designs. These parameters are 1) the shock wave overpressure after the geometric passage (the pressure jump across the incident shock front after the geometric passage), 2) the shock wave Mach number after the geometric passage and 3) the reflected shock pressure (the pressure jump across the reflected shock front from the target location). In the present study, the incident shock overpressures at various monitoring locations after the geometric passage has been compared for different cases. The various measuring locations are shown in the inset in Fig. 8 (a) to

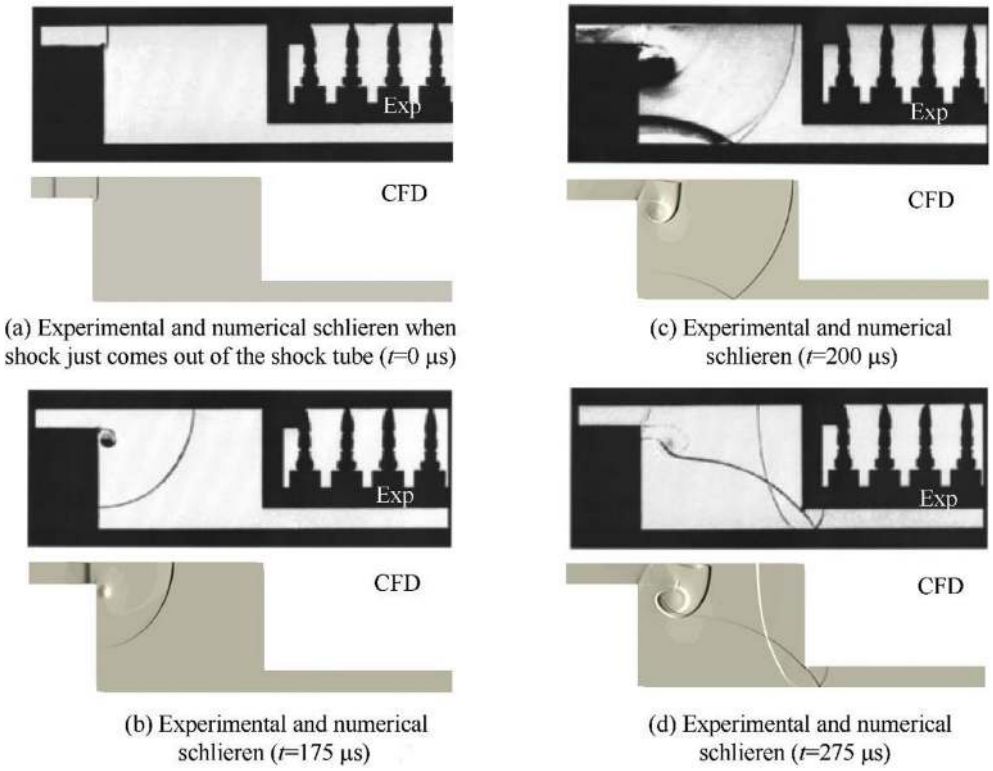

Fig. 7. Comparison of numerical schlieren to experimental schlieren images [15] at various time instants.

8(d). The comparison of shock overpressures for various cases at measuring point-1 (Fig. 8(a)) clearly shows that the pressure jump is reduced with geometric passages compared to the plain shock tube. A similar trend in pressure history can also be observed at various measuring location, as shown in Fig.8 (b) to Fig. 8(d). It is seen from Fig. 8 that, among the various geometric cases, the maximum attenuation in shock strength is produced by case-4 geometry (zig-zag duct with cylinders), which is then followed by case-2 (zig-zag duct) and case-3 (staggered cylinders), respectively. However, it is to be noted that the shock wave attenuation produced by case-2 (zig-zag) and case-3 (staggered cylinder) geometries are not so prominent as case-4. This can be attributed to several factors, such as the variation in shock wave reflections and diffractions, the level of flow obstruction, the variation in shock wave Mach number etc. incurred in various cases. Moreover, it is also seen from Fig. 8 that the cases with geometric passage produce repetitive pressure peaking's at the monitoring locations, which can be linked to the multiple shock wave reflections within the geometric patterns.

Another critical parameter that defines the shock strength is the shock wave Mach number. In the present study, the shock wave Mach number at the downstream side of various geometric passages has been computed and is shown in Fig. 9. The shock Mach number is computed by noting the shock arrival time at various predefined measuring locations along the centerline. It is clearly seen that the shock wave Mach number reduces with the geometric obstructions. Fig. 9 also shows that the maximum reduction in shock wave Mach number is produced with the case-4 passage, and this result in larger reduction in pressure jump across the shock wave, as seen in Fig. 8.

It is well known that the reduction in shock wave Mach number reduces the reflected shock pressure, which is another important parameter for shock attenuation. Fig. 10 shows the area-averaged pressure history at the end wall produced by the reflected shock wave for various cases. It is clearly seen that the reflected shock pressure reduces considerably with all the geometric passage cases considered in the present study. A substantial reduction in reflected shock pressure can be observed with the case-4 passage (zig-zag with cylinders). The zig-zag (case-2) and staggered cylinder (case-3) geometries also show a considerable reduction in reflected shock pressure, as seen from Fig. 10.

A comparison of the percentage reduction in the reflected shock pressure from the plain shock tube case for various cases is shown in Fig. 11. It is clearly seen from Fig. 11 that as much as 63% reduction in reflected shock pressure can be obtained with zig-zag with cylinders geometry (case-4). The zig-zag duct (case-2) and staggered cylindrical obstructions (case-3) produced nearly 34% reduction in reflected pressure jump from the plain shock tube case. Past studies based on geometric passage reported that the effectiveness of shock attenuation increase with blockage area. However, the zig-zag design in the present study produced notable shock attenuation with practically no blockage to the flow area (blockage ratio = 0). A combination of zig-zag with cylinders produced drastic attenuation in shock reflection pressure with a moderate blockage ratio (BR = 0.4). From Fig. 11, it is clearly evident that the various designs proposed in the present study produced prominent shock wave attenuation without much flow obstruction. In order to further understand the physics of the shock wave attenuation with various geometric designs, a detailed investigation on the shock wave reflection and diffraction with the geometric passages has been carried out, as discussed below.

3.2. Shock reflection and refraction characteristics for various designs

This section discusses the shock reflection and diffraction

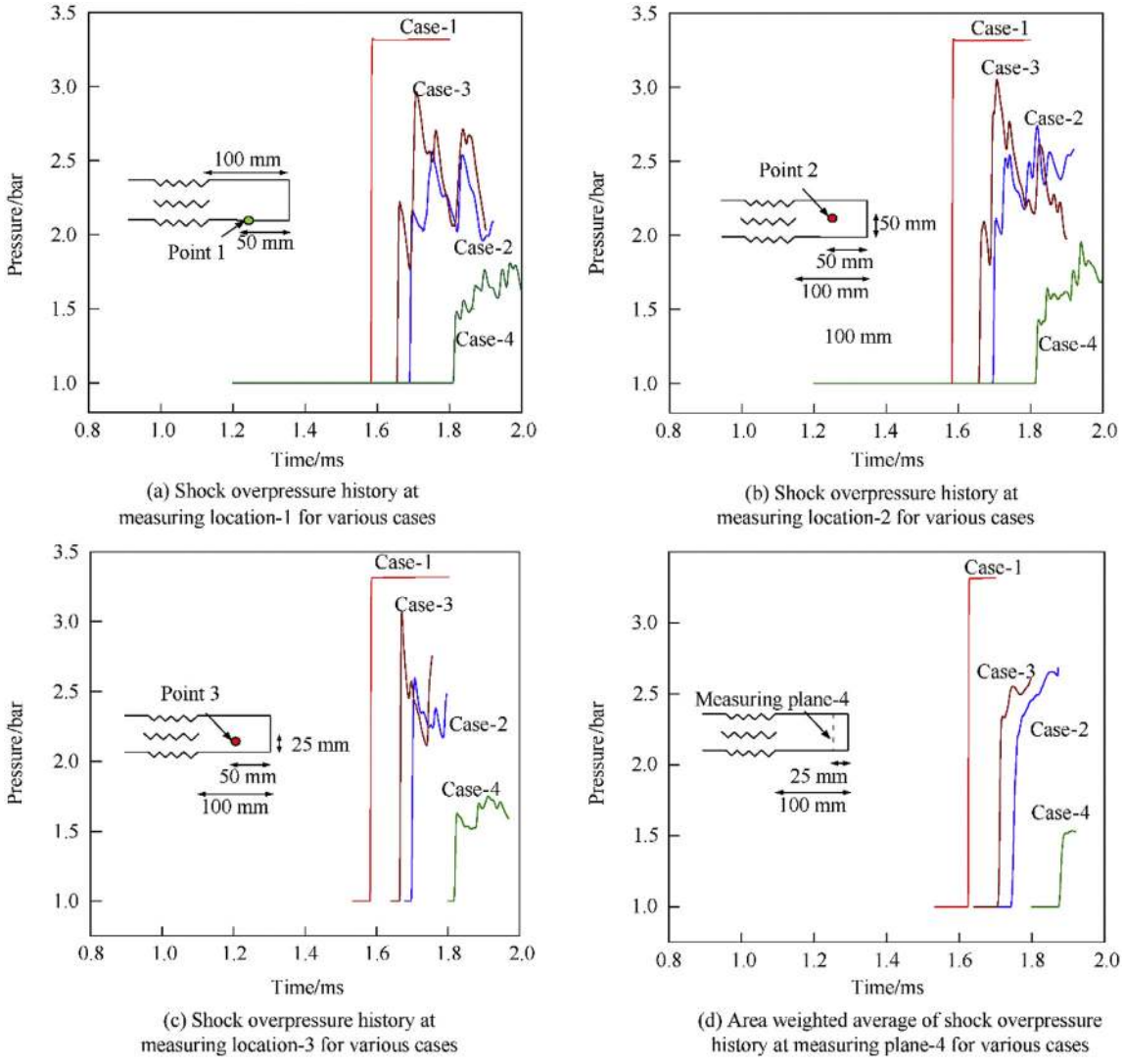

Fig. 8. Pressure histories at different measuring locations for various cases.

characteristics produced by various geometric designs. This section is sub divided into two categories. The first subsection discusses the shock wave reflection with in in the geometric passage and the second subsection discusses the shock reflections and shock overpressure downstream to the geometric passage.

3.2.1. Shock reflection and refraction with in the geometric passage

3.2.1.1. Zig-zag passage (Case-2). Fig. 12 shows the numerical schlieren for the shock tube simulation with zig-zag geometric passage (case-2). It is seen that the initial plane shock wave is split into two waves by the middle wall of the zig-zag duct (Fig. 12 (a)). These waves are referred to as the transmitted shock wave (TSW). In the top wall region of the zig-zag duct, the transmitted shock wave initially sees a compression corner, whereas, in the bottom wall region of the zig-zag duct, the transmitted shock wave sees an expansion corner. Hence, the foot of the shock front at the top wall region undergoes a shock wave reflection, whereas at the bottom wall region, the shock wave undergoes a shock diffraction process, as clearly seen from Fig. 12 (a). In the upper side of the middle wall, the transmitted shock wave sees an expansion corner and results in shock wave diffraction. On the other hand, the lower side of the middle wall acts as a compression corner and produce shock wave reflection. These results can be clearly seen in Fig. 12 (a). It can be seen from the numerical schlieren (Fig. 9(b)) that the reflected shock wave initially exhibits a simple Mach reflection (SMR) with three shock discontinuities meeting at a single point. A detailed description of the various shock wave reflection patterns produced by moving shock front along wedges of various angles (commonly known as pseudo-steady reflections) can be found in the monograph by Ben-Dor [30]. Another thing to notice is that as the transmitted shock front propagates downstream, the reflected shock wave grows and moves upstream. This can be clearly noticed from Fig. 12(c). The reflected shock waves from the top and middle walls eventually interact and coalesce to form a secondary shock wave (SSW) moving in the upstream direction, as clearly seen from Fig.12 (d) to Fig. 12 (h).

As the transmitted shock wave moves to the second turn of the zig-zag duct, shock wave diffraction happens at the top wall and shock wave reflection happens at the bottom wall, as clearly seen from Fig. 12(d). This is opposite to what been seen in the first turn of the zig-zag duct. This is because, in the second turn the top wall acts as an expansion corner and the bottom wall acts as compression corner. This reversal in shock wave reflection and diffraction can also be seen in the middle wall. As a consequence of this, the

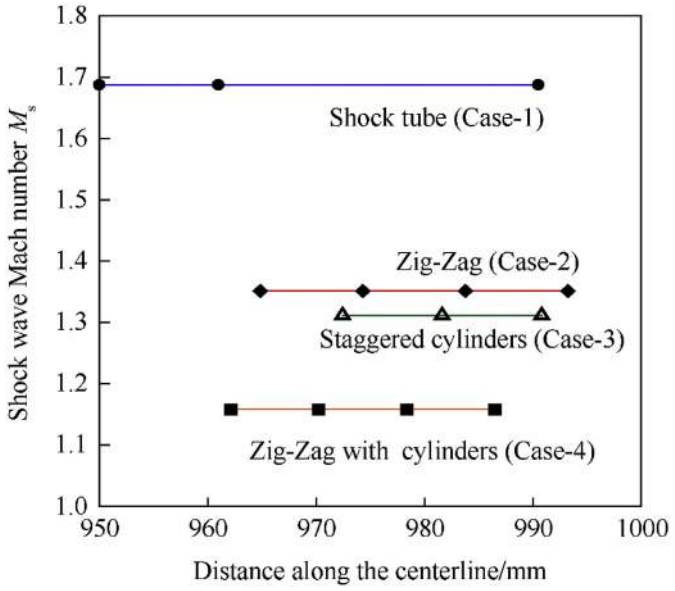

Fig. 9. Shock wave Mach number (M_s) for various cases.

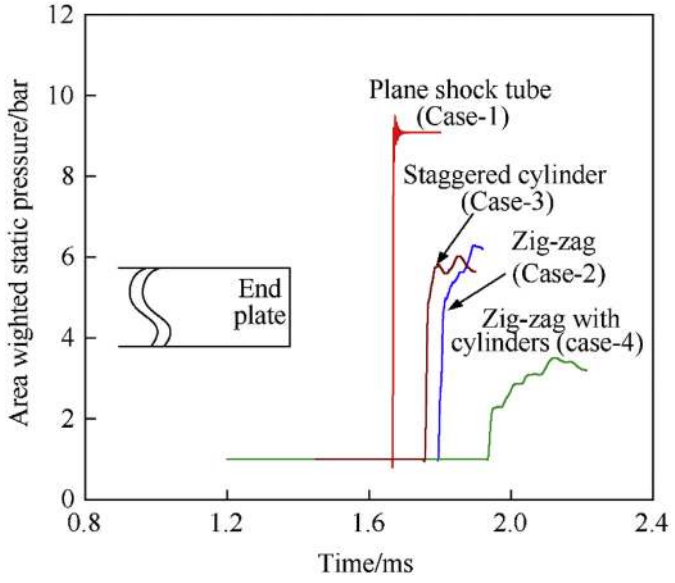

Fig. 10. Area weighted pressure histories at the end plate for various cases.

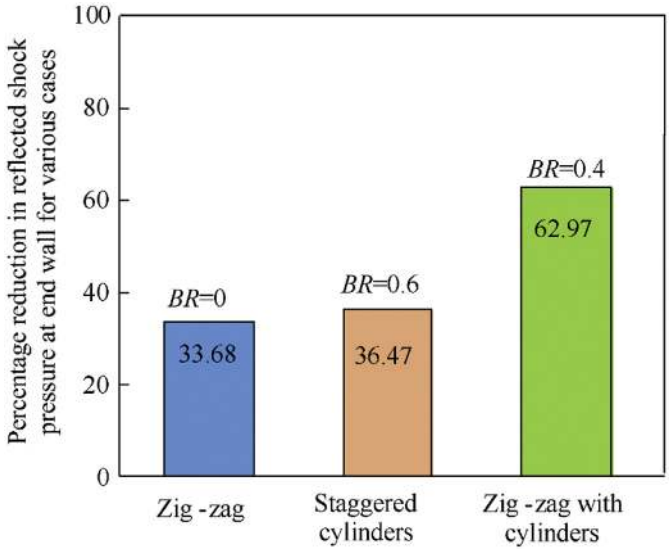

Fig. 11. Reduction in reflected shock pressure for various cases from the plain shock tube case at the end wall.

reflected shock wave from the bottom wall eventually interacts with the reflected shock from the lower portion of the middle wall, as seen in Fig. 12 (d). This leads to a complex multiple shock reflection pattern in the bottom wall region as shown in Fig. 12 (e). A similar multiple shock wave reflection can also be observed in the upper side of the middle wall region. As the transmitted shock front moves further to the third turn of the zig-zag duct, the top wall again becomes a compression corner and the bottom wall turns to an expansion corner. Now the shock wave reflection happens at the top wall and at the lower portion of the middle wall, whereas, shock wave diffraction happens at the bottom wall and at the upper portion of the middle wall (Fig. 12 (f)). In the third turn, the reflected shock waves move toward each other in the top wall region and in the lower portion on the middle wall, as clearly observable from Fig. 12(g). The reflected shock waves eventually interact and result in multiple shock reflections at the top wall and at the bottom side of the middle wall, as seen in Fig. 12 (h).

It is thus seen from Fig. 12 that the transmitted shock wave undergoes shock wave reflection and diffraction as it moves along the zig-zag passage. As the primary shock front moves from one turn to the other turn of the zig-zag duct, the shock reflection process swaps to shock diffraction, and the shock diffraction process swaps to the shock reflection process. This interchanging of shock reflection to shock diffraction and vice versa continuous cyclically as it moves from one turn to the other. As a result of this, a portion of the primary shock wave energy is lost in the multiple shock reflections and shock diffractions. The main advantages of the zig-zag structure compared to the previously studied geometric blockages are that the multiple shock reflection and diffraction can be produced without much solid obstructions placed in the flow area. A large number of solid blockages placed in the flow field increase the weight of the protective structure and in this regard the zig-zag structure provides a better design.

3.2.1.2. Staggered cylinders (Case-3). For case-3 design, the moving shock wave over the cylindrical body results in purely unsteady shock reflection [30], as shown in Fig. 13 (a) and 13 (b). The reflected shock wave from the cylinders eventually coalesces with each other and forms a near plane secondary shock front propagating in the upstream direction (SSW1), as shown in Fig. 13(c) to 13(h). In the wake of the cylinder, the transmitted shock wave diffracts and curves out as shown in Fig. 13(c). The diffracted shock waves from the adjacent cylinders interact with each other and results in further reflection, as shown in Fig. 13(d). As the transmitted shock wave moves further downstream, it interacts with the second column of cylinders. The transmitted shock wave again undergoes shock wave reflection in the forward side of the cylinder and shock wave diffraction in the rearward side of the cylinder. This can be clearly noticed from Fig. 13 (e) and 13 (f). The reflected shock wave from the second column of cylinder grows and eventually interacts with the diffracted shock wave from the first column of cylinders, as shown in Fig. 13 (f). These two shock waves coalesce and form a secondary shock front (SSW2) as shown in Fig. 13 (g). Fig. 13 (h) shows that the shock reflections from multiple cylinders eventually produce multiple secondary shock waves (marked as SSW1 and SSW2) which propagate in the upstream direction. The shock attenuation for the staggered cylindrical case can thus be

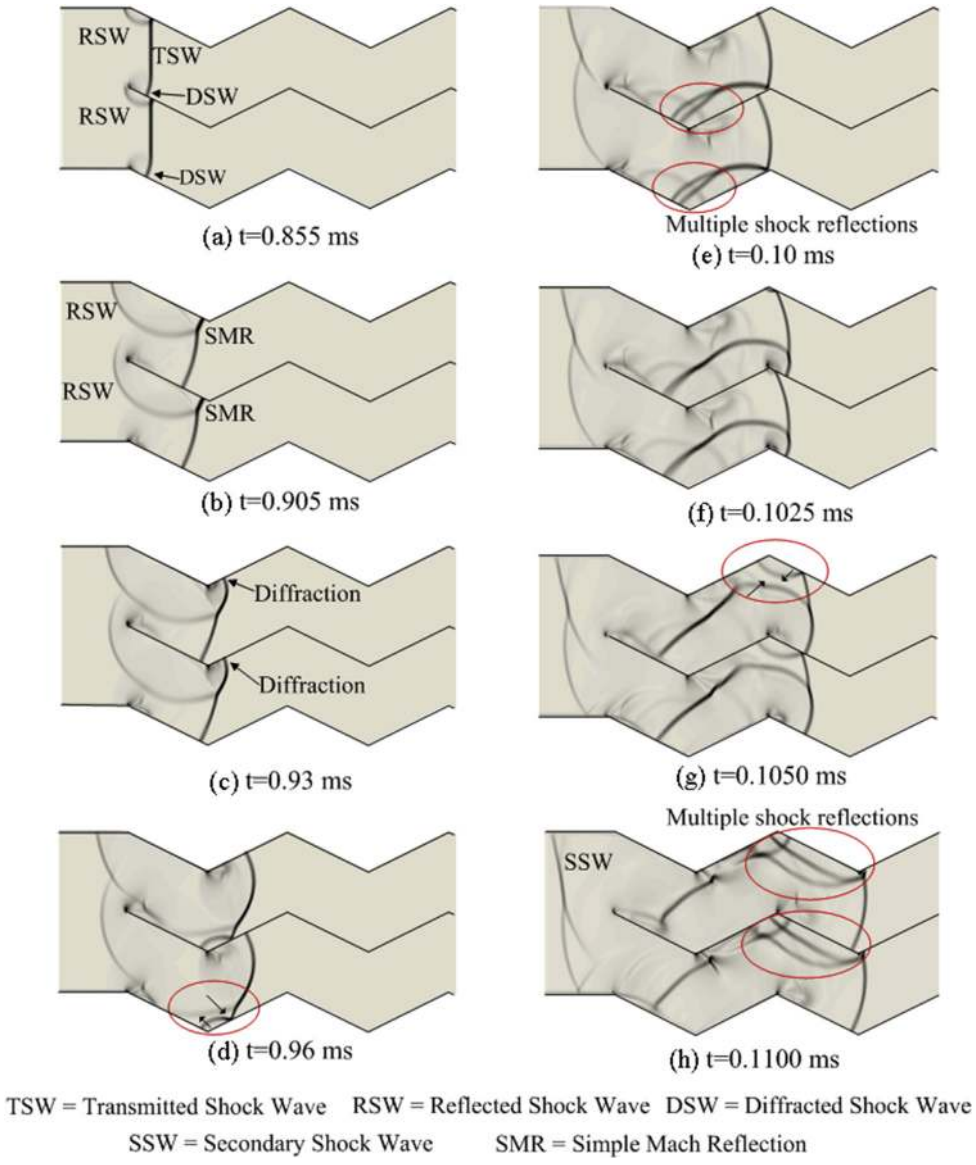

Fig. 12. Numerical schlieren for zig-zag geometric passage (case-2) at various time instants.

mainly attributed to the flow obstruction and the shock wave diffraction and reflection produced by the cylindrical obstructions. However, the main disadvantage of such design is the localized pressure peaking's due to multiple shock reflections.

3.2.1.3. Zig-zag passage with cylinders (Case-4). Fig. 14 shows the numerical schlieren for the case-4 geometric passage (zig-zag passage with cylinders). It should be noted that case-4 is an extension of case-2 with additional cylindrical obstructions. Hence, the initial shock structures for case-4 will be the same as that of case-2 with shock wave diffraction and shock wave reflection happening at the foot of the shock wave, as clearly seen in Fig. 14(a). As the shock front moves further downstream, it encounters the cylindrical obstructions and results in unsteady shock wave reflection from the cylindrical surface, as shown in Fig. 14. (b). This reflected shock wave grows and interacts with the ziz-zag wall, resulting in multiple shock reflections as shown in Fig. 14 (c). The reflected shock waves from the first leg of the zig-zag duct and the first column of cylindrical blockages eventually coalesces and form a secondary shock wave, as shown in Fig. 14 (d) to 14 (f). The transmitted shock wave undergoes multiple reflections as it passes through the subsequent portion of the zig-zag duct and the cylindrical blockages, as shown in Fig. 14(e). The reflected shock waves in each pass coalesces together to form multiple secondary shock waves, as shown in Fig. 14 (f). It is thus clear from the numerical schlieren that the presence of cylindrical obstructions in case-4 produces additional shock wave reflection compared to case-2. This results in more diffusion of initial shock wave energy and aids the shock attenuation process. Moreover, the flow obstructions retard the mass motion velocity behind the shock wave, which also helps in reducing the reflected shock pressure. Hence, larger shock wave attenuation happens with the case-4 passage, which is also evident in Fig. 8.

3.2.2. Shock reflection and refraction characteristics downstream to the geometric passage

It is seen from the numerical schlieren images that the shock attenuation strategies based on geometric passages result in complex shock reflections and multiple shock wave interactions. As a result of this, the shock front after passing through the geometric

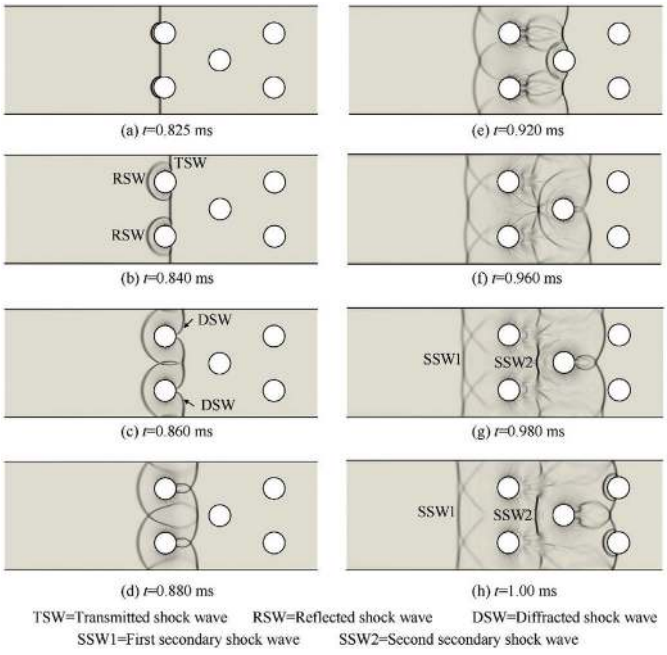

Fig. 13. Numerical schlieren for staggered cylinders (case-3) at various time instants.

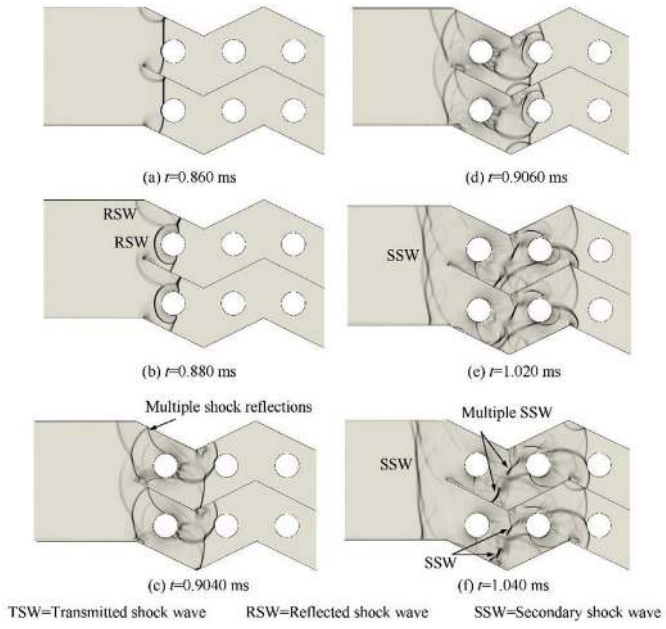

Fig. 14. Numerical schlieren for zig-zag with staggered cylinders (case-4) at various time instants.

obstructions will no longer be plane. This can be clearly seen from Fig. 15, which shows the numerical schlieren depicting the shock structures for various cases after passing through the geometrical passages. The transmitted shock wave from the geometric passage exhibits a complex reflected shock wave structure with the interaction of multiple Mach reflection structures, as shown in Fig. 15. It is well known that the interaction of multiple shock structures increases the pressure. However, the pressure contours (Fig. 16) show that even with multiple shock front interactions after the geometric passage, the maximum pressure rise is still below than that produced by the plain shock tube case. A reduction in shock

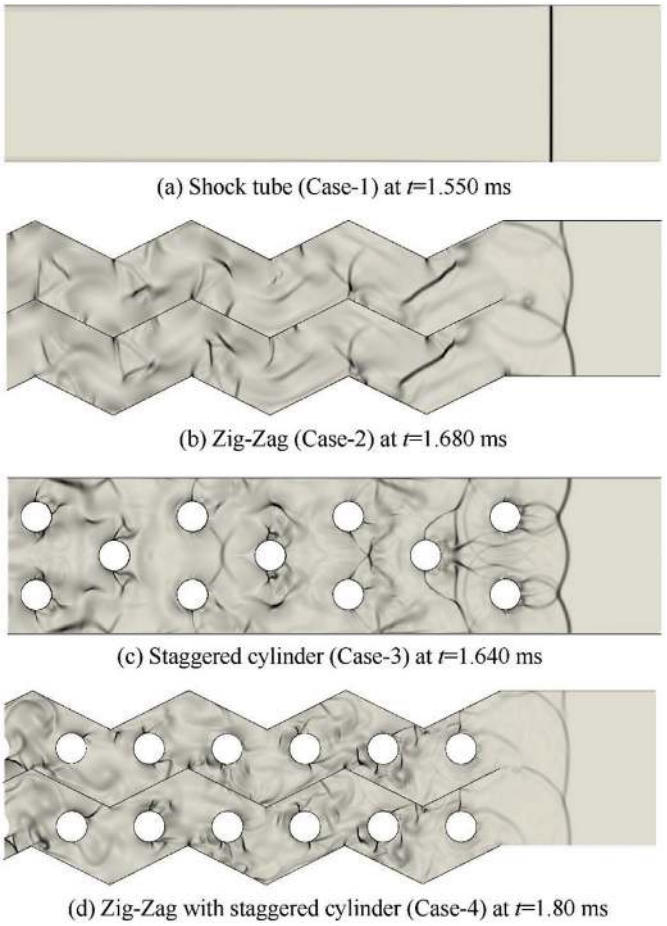

Fig. 15. Numerical schlieren showing the transmitted shock front after passing through various geometric passages.

overpressure even after interaction of multiple shock fronts clearly indicates that the incident shock after the geometric passage attenuates significantly. It is also seen from the numerical schlieren (Fig. 15) that the multiple shock interactions are more prominent for the staggered cylindrical passage (case-3). The cylindrical geometry results in more prominent shock diffraction and the diffracted shock from the adjacent cylinders interact with each other resulting in multiple shock interactions. This effect is not so prominent in other geometric passage cases. This can also be noticed from the pressure histories for various cases shown in Fig. 8. The pressure histories show that among the various geometric passage cases, the maximum pressure jump across the shock front happens for the staggered cylinder case. The pressure histories also show multiple pressure jumps for the cases with geometric passages. The multiple pressure rises can be attributed to the multiple shock waves produced due to shock-shock interactions, as clearly seen in Fig. 15.

It is clearly seen from Fig. 9 that the shock wave speed reduces with the geometric obstructions. This is due to the attenuation of shock speed produced by the obstruction and the energy spent on the multiple shock reflections and diffractions in the passage area. A qualitative picture of the reduction in shock speed for various cases can also be seen from the pressure contours, shown in Fig. 16. In Fig. 16, the pressure contours for all the cases at a common time instant have been shown. The contours clearly show that, for a particular time instant, the maximum shock propagation distance can be found for the shock tube cases whereas, the minimum shock

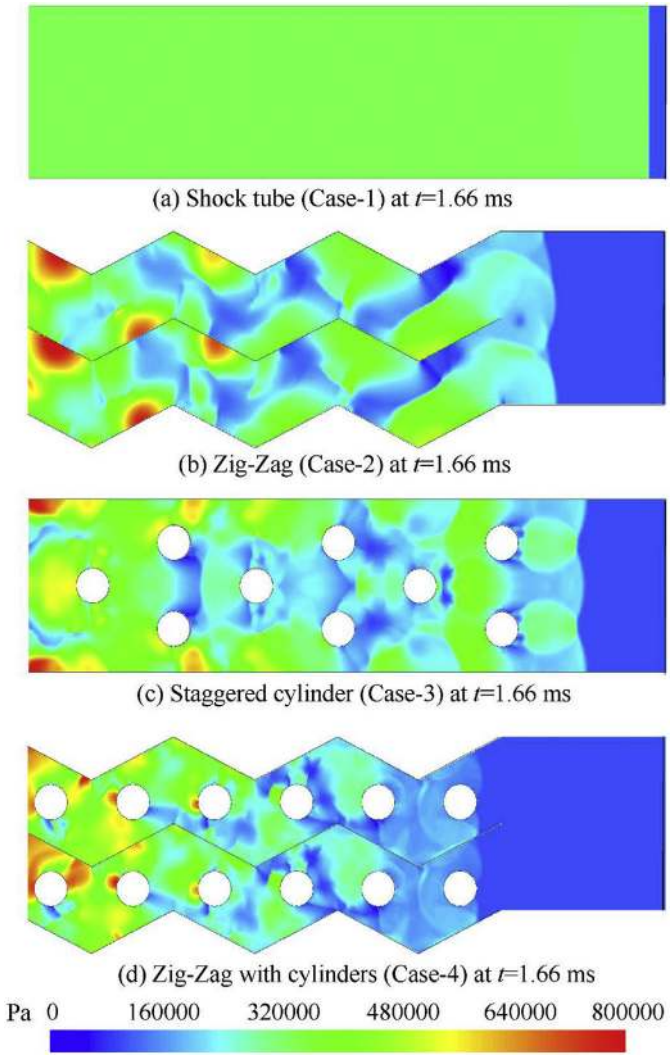

Fig. 16. Pressure contours for different cases at t = 1.66 ms.

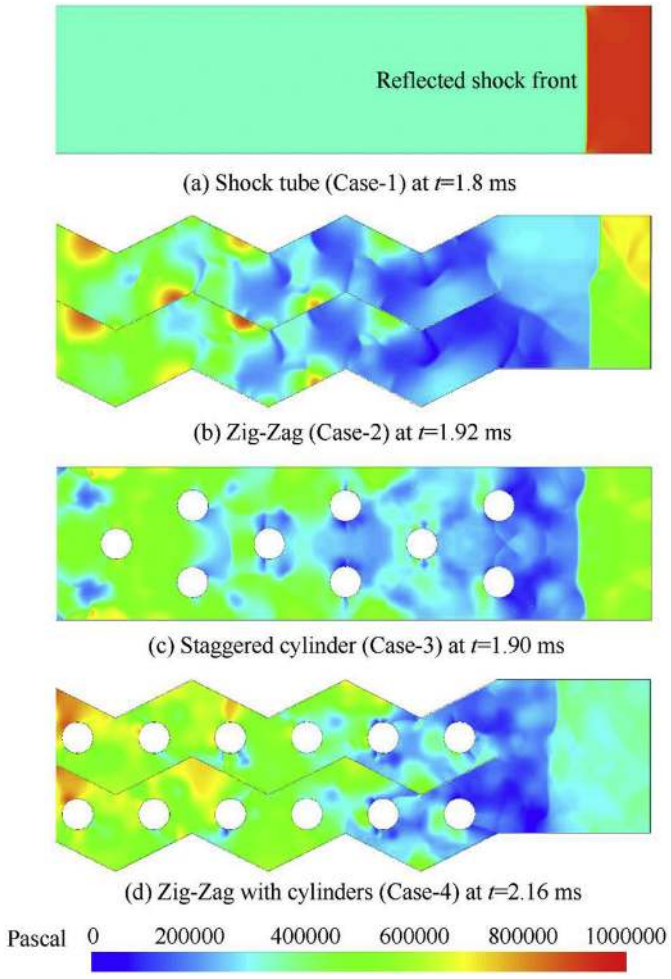

Fig. 17. Pressure contours for different cases after shock reflection.

propagation distance can be found for the zig-zag with cylinders case (case-4). This clearly shows that the shock propagation speed is much less for the zig-zag passage with cylinders compared to plain shock tube case. The pressure contours also show a non-uniform pressure distribution behind the shock front for the cases with the geometric passages, with minimum pressure rise seen for case-4 passage. This non-uniform pressure distribution is due to the multiple shock wave interaction.

The reduction in shock speed due to geometric obstructions reduces the shock wave Mach number which in turn reduces the reflected shock pressure, as shown in Fig. 10. A qualitative picture of this is shown in Fig. 17, which shows the pressure contours for various cases after the shock wave reflection. It is clearly seen that a non-uniform pressure distribution behind the reflected shock can be found for all the cases with geometric passages. Nevertheless, the pressure rise for all the geometric cases is far below than that produced with plain shock tube.

It is thus clear from the pressure histories (section 3.1) and pressure contours (section 3.2) that the new geometric designs presented in the current study produces excellent shock attenuation characteristics, particularly the reflected shock pressure. It should also be noted that the new geometric designs possess several advantages over many of the past geometric obstruction designs for shock attenuation. The major advantage comes from the fact that the geometric area blockage produced by the new designs (especially the zig-zag case) is considerably low. This will help in reducing the quantity of the structural materials required for the design and hence reduces the overall weight of the protective structure. Moreover, the hollow spaces in the new designs can be utilized to insert shock absorbing materials like poly urethane foams. For example, the zig-zag structure can be sandwiched with polyurethane foams and this can enhance the shock attenuation by the combined action of shock reflection and shock absorption. On the other hand, the major disadvantage of the present design is the localized pressure peaks produced by multiple shock interactions downstream to the geometric passage. Nevertheless, it is found that even with multiple shock interactions the shock overpressure is comparatively lesser that the un obstructed shock wave.

4. Conclusions

The present study compares the effectiveness of shock wave attenuation produced by three different geometrical designs. In the first design, which is a zig-zag passage, the incident shock wave encounters a compression corner at the top wall of the zig-zag duct, resulting in shock wave reflection, and an expansion corner at the bottom wall, resulting in shock wave diffraction. The alternatively changing slope of the zig-zag wall changes the shock reflection to shock diffraction and vice versa as the shock propagates along the

passage, resulting in multiple shock reflection patterns. The second geometric design, which is the cylindrical blockages arranged in a staggered fashion, leads to shock wave reflection in the forward half of the cylindrical surface and shock wave diffraction in the rearward half. The flow blockage produced by the cylindrical geometry also reduces the bulk motion velocity behind the shock wave. The third design, which is a combination of zig-zag passage with cylindrical obstructions, produces alternate shock wave reflection and diffraction along the zig-zag wall as well as shock reflection and diffraction from cylindrical obstructions. This combined effect leads to a drastic reduction in shock strength. It is found that the zig-zag duct with cylindrical obstructions produced a reduction of nearly 63% in the reflected shock pressure compared to the plain shock tube case, whereas, the other two designs reduced the reflected shock pressure by nearly 34%.

Declaration of competing interest

The authors declare that they have no known competing financial interests or personal relationships that could have appeared to influence the work reported in this paper.

Acknowledgements

This research project is funded by the INSPIRE research grant from the Department of Science and Technology (DST), India.

References

[1] Needham CE. Blast waves. Berlin, Heidelberg: Springer; 2010.
[2] Hetherington J, Smith P. Blast and ballistic loading of structures. CRC Press; 2014.
[3] Wightman JM, Gladish SL. Explosions and blast injuries. Ann Emerg Med 2001;37(6):664–78.
[4] Prat NJ, Daban JL, Voiglio EJ, Rongieras F. Wound ballistics and blast injuries. J Vis Surg 2017;154(1):9–12. https://doi: 10.1016/j.jviscsurg.2017.07.005.
[5] Elder GA, Stone JR, Ahlers ST. Effects of low-level blast exposure on the nervous system: is there really a controversy? Front Neurol 2014;5:269. https://doi: 10.3389/fneur.2014.00269.
[6] Sawyer TW, Josey T, Wang Y, Villanueva M, Ritzel DV, Nelson V, et al. Investigations of primary blast-induced traumatic brain injury. Shock Waves 2018;28:85–99. https://doi: 10.1007/s00193-017-0756-2.
[7] Hicks RR, Fertig SJ, Desrocher RE, Koroshetz WJ, Pancrazio JJ. Neurological effects of blast injury. J Trauma 2010;68(5):1257–63. https://doi:10.1097/TA.0b013e3181d8956d.
[8] Glass II, Sislian JP. Nonstationary flows and shock waves. Clarendon Press; 1994.
[9] Dosanjh DS. Interaction of grids with traveling shock waves. NACA TN 1956;3680.
[10] Britan A, Igra O, Ben-Dor G, Shapiro H. Shock wave attenuation by grids and orifice plates. Shock Waves 2006;16:1–15. https://doi:10.1007/s00193-006-0019-0.
[11] Britan A, Karpov AV, Vasilev EI, Igra O, Ben-Dor G, Shapiro E. Experimental and numerical study of shock wave interaction with perforated plates. J Fluid Eng 2004;126(3):399–409. https://doi.org/10.1115/1.1758264.
[12] Ohtomo F, Ohtani K, Takayama K. Attenuation of shock waves propagating over arrayed baffle plates. Shock Waves 2005;14:379–90. https://doi.org/10.1007/s00193-005-0282-5.
[13] Berger S, Sadot O, Ben-Dor G. Experimental investigation on the shock-wave load attenuation by geometrical means. Shock Waves 2009;20:29–40. https://doi.org/10.1007/s00193-009-0237-3.
[14] Chaudhuri A, Hadjadj A, Sadot O, Ben-Dor G. Numerical study of shock-wave mitigation through matrices of solid obstacles. Shock Waves 2012;23:91–101. https://doi.org/10.1007/s00193-012-0362-2.
[15] Igra O, Wu X, Falcovitz J, Meguro T, Takayama K, Heilig W. Experimental and theoretical study of shock wave propagation through double-bend ducts. J Fluid Mech 2001. https://doi:10.1017/S0022112001004098.
[16] Baer M. A numerical study of shock wave reflections on low density foam. Shock Waves 1992;2:121–4. https://doi.org/10.1007/BF01415901.
[17] Britan A, Shapiro H, Liverts M, Ben-Dor G, Chinnayya A, Hadjadj A. Macro-mechanical modeling of blast wave mitigation in foams. Part I: review of available experiments and models. Shock Waves 2012;23:5–23. https://doi:10.1007/s00193-012-0417-4.
[18] Petel OE, Ouellet S, Higgins AJ, Frost DL. The elastic-plastic behaviour of foam under shock loading. Shock Waves 2013;23:55–67. https://doi: 10.1007/s00193-012-0414-7.
[19] Sommerfeld M. The unsteadiness of shock waves propagating through gas–particle mixtures. Experiments in fluids. 1985. https://doi.org/10.1007/BF00265101.
[20] Bakken J, Slungaard T, Engebretsen T, Christensen SO. Attenuation of shock waves by granular filters. Shock Waves 2003;13:33–40. https://doi.org/10.1007/s00193-003-0180-7.
[21] Sembian S, Liverts M, Apazidis N. Attenuation of strong external blast by foam barriers. Phys Fluids 2016;28(9). https://doi: 10.1063/1.4963243.
[22] Kitagawa K, Yasuhara M, Takayama K. Attenuation of shock waves propagating in polyurethane foams. Shock Waves 2006;15:437–45. https://doi.org/10.1007/s00193-006-0042-1.
[23] Sounik D, Gansen P, Clemons J, Liddle J. Head-impact testing of polyurethane energy-absorbing (EA) foams. Paper SAE Tech 1997. https://doi:10.4271/970160.
[24] Song B, Chen WW, Dou S, Winfree NA, Kang JH. Strain-rate effects on elastic and early cell-collapse responses of a polystyrene foam. Int J Impact Eng 2005;31:509–21. https://10.1016/j.ijimpeng.2004.02.003.
[25] Hajek R, Foglar M, Fladr J. Influence of barrier material and barrier shape on blast wave mitigation. Construct Build Mater 2016;120:54–64. https://10.1016/j.conbuildmat.2016.05.078.
[26] Foglar M, Hajek R, Kovar M, Stoller J. Blast performance of RC panels with waste steel fibers. Construct Build Mater 2015;94:536–46. https://10.1016/j.conbuildmat.2015.07.082.
[27] Taha A, Zahran MS, Gao Z. Mitigation of the blast load effects on a building structure using newly composite structural configurations. Defence Technology; 2020. https://doi.org/10.1016/j.dt.2020.03.002.
[28] Igra O, Falcovitz J, Houas L, Georges J. Review of methods to attenuate shock/blast waves. Prog Aero Sci 2013;58:1–35. https://10.1016/j.paerosci.2012.08.003.
[29] Reddy KPJ, Sharath N. Manually operated piston-driven shock tube. Curr Sci 2013;104:172–6. https://www.jstor.org/stable/24089380.
[30] Ben-Dor G. Shockwave reflection phenomenon, vol. 2. Springer; 2007.
[31] Settles GS. Schlieren and shadowgraph techniques, vol. 1. Springer; 2001. https://doi.org/10.1007/978-3-642-56640-0.